CEA Comité Español de Automática
XLVI JORNADAS AUTOMÁTICA CARTAGENA 2025
UNIVERSIDADE DA CORUÑA

Jornadas de Automática

Modeling and Fuzzy Control of the *Unimation PUMA 560* Shoulder Actuator Position

Fernández-Infante Sánchez-Camacho, Alejandro[a,*], Santos Peñas, Matilde[b], Sierra-García, Jesús Enrique[c]

[a] *Computer Engineering School, Complutense University of Madrid, 28040, Madrid, Spain.*
[b] *Institute of Knowledge Technology, Complutense University of Madrid, 28040, Madrid, Spain.*
[c] *Department of Electromechanical Engineering, University of Burgos, 09006, Burgos, Spain.*

To cite this article: Fernández-Infante Sánchez-Camacho, Alejandro, Santos Peñas, Matilde, Sierra-García, Jesús Enrique. 2025 Modeling and Fuzzy Control of the *Unimation PUMA 560* Shoulder Actuator Position. Jornadas de Automática, 46. https://doi.org/10.17979/ja-cea.2025.46.12275

Abstract

This work investigates the position control of the *Unimation PUMA 560* shoulder joint actuator using a cascaded control architecture, comprising an inner velocity control loop and an outer position control loop. A *Mamdani*-type fuzzy PD+I controller is implemented in the inner loop to avoid the complexity of a full fuzzy PID scheme rule set, while a linear proportional controller is employed in the outer loop. The system model captures key nonlinear behaviours arising from variable loads and friction. Simulations are conducted under both nominal conditions and a 20 N·m disturbance torque introduced to emulate gravitational effects, with tracking performance evaluated using a combination of time-domain metrics and quantitative indicators.

Keywords: cascade control, fuzzy logic, *PUMA 560* manipulator, F-PD+I controller, trajectory tracking.

Modelado y control borroso de la posición del actuador del hombro del *Unimation PUMA 560*

Resumen

Este trabajo investiga el control de posición del actuador de la articulación del hombro del *Unimation PUMA 560* mediante una arquitectura de control en cascada, que comprende un lazo interno de control de velocidad y un lazo externo de control de posición. En el lazo interno se implementa un controlador borroso PD+I tipo *Mamdani* con el fin de evitar la complejidad asociada al conjunto de reglas de un PID borroso, mientras que en el lazo externo se emplea un regulador proporcional lineal. El modelo del sistema captura comportamientos no lineales clave derivados de cargas variables y fricción. Se realizan simulaciones tanto en condiciones nominales como ante un par perturbador de 20 N·m introducido para emular efectos gravitacionales, evaluando el rendimiento del seguimiento por medio de una combinación de métricas en el dominio del tiempo e indicadores cuantitativos.

Palabras clave: control en cascada, lógica borrosa, manipulador *PUMA 560*, controlador F-PD+I, seguimiento de trayectorias.

1. Introduction

Over the years, robotics has emerged as a key research field, driven by the need for machines to perform tasks that are either too dangerous or physically demanding for humans. In this context, the introduction of the *Programmable Universal Machine for Assembly* (*PUMA*) in 1978 marked a significant milestone in robotic design and programming. Position and velocity control are essential in robotic systems, especially for joint movement. However, controlling each joint as an independent system presents challenges due to disturbance torques such as gravity, friction and coupling effects. A widely adopted solution is the implementation of a nested control loop architecture (Corke, 2007), where the outer loop governs position and the inner loop regulates velocity, ensuring accurate tracking performance in the presence of external disturbances.

Although the PID controller remains an industry stan-

*Author for correspondence: alejaf28@ucm.es

dard, several fuzzy logic-based control strategies have been proposed to overcome its limitations (Alavandar and Nigam, 2008; Singh et al., 2020; Usoro et al., 2017; Sierra-Garcia and Santos, 2024). Fuzzy logic controllers (FLCs) do not rely on an explicit mathematical model of the system and are often less computationally intensive (Zadeh, 1996). This study proposes the application of a cascaded control strategy to the shoulder joint actuator during a trajectory.

This paper is structured as follows: Section 2 provides an overview of the physical system and the mathematical modelling of the actuator. Section 3 details the design of the fuzzy controller. Section 4 presents and discusses the experimental results. Finally, Section 5 summarizes the key findings and outlines potential directions for future research.

2. Manipulator model

The *Unimation PUMA 560* manipulator features six degrees of freedom (DOF), enabling a high level of versatility. This configuration is achieved through an *Euler* wrist — comprising the last three DOFs — in combination with the waist, shoulder, and elbow joints. Its workspace, however, is constrained by the range of motion allowed by each individual joint, as well as by its *Denavit–Hartenberg* (D-H) parameters.

Despite this, accurately replicating the robotic arm model remains a challenge, as noted in the literature. Therefore, to ensure consistency with the simulation, the parameters and conventions proposed in (Corke and Armstrong-Helouvry, 1994; Corke, 2007) are adopted as the reference.

2.1. Manipulator kinematics

As mentioned in (Barrientos et al., 2007), the kinematics of the robot aims to study the spatial relationships of its movements, disregarding the physical forces. First, the reference system must be established at its ready pose ($\vec{q_r}$), as illustrated in Figure 1(a). The goal is to define the parameters of each link/joint pair — specifically those associated with the second link (q_2) in this case. These parameters include a link length (d_2) of 0, a link offset (a_2) of 0.4318 and a link twist (α_2) of 0 (Figure 1(b)).

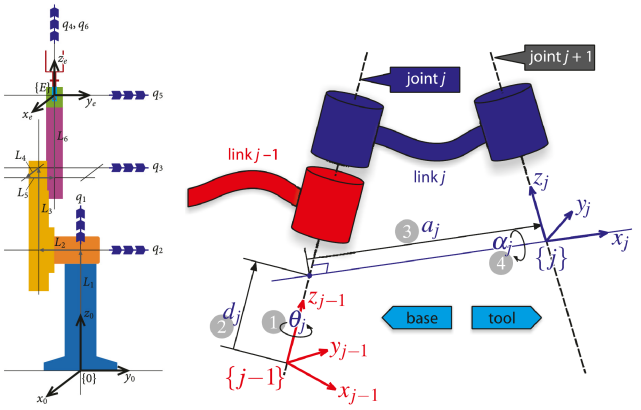

(a) $\vec{qr}$ (b) D-H notation for a revolute pair

Figure 1: Reference system and parametrization Corke (2007)

The motion kinematics of a manipulator (Barrientos et al., 2007) is typically defined in cartesian space. However, since the control of this movement occurs in joint space, it is essential to establish the relationships between both spaces.

In this work, trajectory planning in joint space will focus on trajectories of the Linear Segment with Parabolic Blend (LSPB) type. In general terms, this scalar trajectory smoothly transitions from an initial position, θ_i, to a final position, θ_{i+1}. Known as a trapezoidal trajectory due to the shape of the velocity curve over time, it is widely used in industrial motor drives and consists of the following three segments:

- From 0 to α: the trajectory follows a quadratic polynomial, resulting in a linear increase in velocity (ramp).
- From α to $T - \alpha$: during the blend time τ, the trajectory transitions to a linear function, representing a constant velocity segment that continues until $T - \tau$.
- From $T - \alpha$ to T: the trajectory switches back to a quadratic polynomial, ensuring smooth deceleration until the final position is reached.

2.2. Manipulator dynamics

The dynamic behavior of an n-joint robot is governed by the 2nd order differential Equation (1). Commonly referred to as state-space equation, it connects the forces exerted on the robot with its motion, specifically relating the position to the torques applied by the actuators to each joint. Identifying the parameters of the shoulder actuator will be crucial for implementing nested control (Barrientos et al., 2007; Corke, 2007).

$$\tau = M(q)\ddot{q} + C(q,\dot{q})\dot{q} + \vec{f}(\dot{q}) + \vec{g}(q) \tag{1}$$

On one hand, the robot's inertial matrix $M \in \mathbb{R}^{n\times n}$ $(kg.m^2)$ represents the change in the system's state of motion, meaning that it relates τ to $\ddot{q}$ for a given q. On the other hand, $\vec{g} \in \mathbb{R}^n$ represents the gravitational torques $(m.s^2)$ while $C \in \mathbb{R}^{n\times n}$ symbolizes the deviation in movement due to its rotational component (Coriolis and centripetal forces). Finally, $\vec{f} \in \mathbb{R}^n$ is nothing more than the vector representing the torque due to both viscous (b) and Coulomb (f_c) friction of each motor in the joints. With all of this, the force tensor associated with the joint coordinates $\tau \in \mathbb{R}^n$ $(N.m)$ is defined (Corke, 2007).

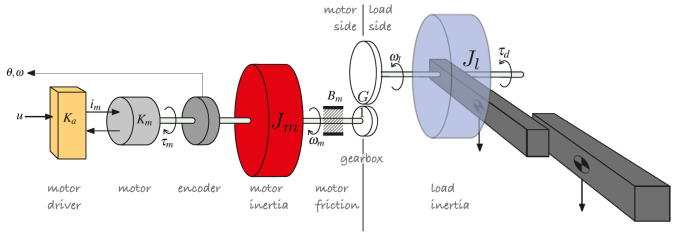

Figure 2: Robot joint schematic Corke (2007)

Therefore, by defining a joint as shown in Figure 2 and knowing that the transconductance (K_a) in the shoulder joint of the manipulator is equal to 0.449 $A.V^{-1}$, it can be stated that the goal of its control is to generate, from a given trajectory represented as $(q, \dot{q}, \ddot{q})$, the control voltage u to be applied in the actuator such that the evolution of the joint closely tracks the reference by using well-established control theory techniques.

When the rotor spins, a voltage V_b is induced, which is directly proportional to the angular velocity ω and is known as the back electromotive force (EMF). This can be expressed as follows:

$$V_b(s) = K_b\omega(s) \tag{2}$$

Note that the motor torque and back EMF constants are equal, that is, $K_m = K_b$. By applying Kirchhoff's second law, the differential Equation of the rotor circuit can be defined as:

$$V_a(s) = (L_a s + R_a)i_a(s) + V_b(s) \tag{3}$$

On the other hand, the motor generates torque proportional to the product of the magnetic flux ϕ and the field current i_f. If i_f is assumed to be constant, ϕ becomes constant, and the torque is directly proportional to the armature current i_a flowing through the rotor (commonly referred to as an armature-controlled DC motor). So, by applying Newton's second law:

$$\tau_m(s) = (J_m s + B_m)\omega(s) + \tau_d(s) = K_m i_a(s) \tag{4}$$

$$i_a(s) = \frac{V_a(s) - V_b(s)}{L_a s + R_a} \tag{5}$$

τ_m is used by the actuator to overcome inertia and friction, accounting for the effects of the link and joint, as well as those of the motor and transmission. These combined effects are referred to as disturbance torques, denoted by τ_d.

$$\omega(s) = \frac{\tau_m(s) - \tau_d(s)}{J_m s + B_m} \tag{6}$$

This is how the transfer function $G_2(s)$, which relates the armature voltage V_a to the rotational speed of the shaft ω and has two poles, is obtained.

$$\frac{\omega(s)}{V_a(s)} = \frac{K_m}{(Las + R_a)(J_m s + B_m) + K_m K_b} \tag{7}$$

As can be seen in Figure 3, by combining the electrical and mechanical equations presented above the DC motor state-space model is obtained, where the input is the applied voltage V_a and the output is the rotational speed ω of the shaft.

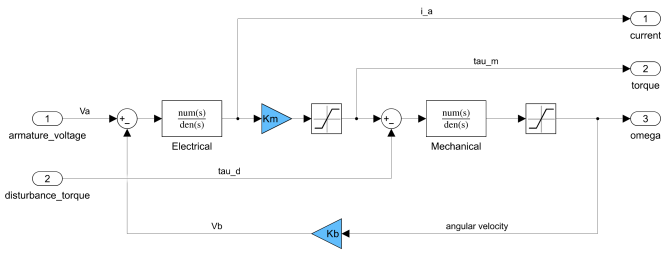

Figure 3: Armature-controlled DC motor model

3. Control architecture

When controlling a robotic manipulator, the system is often modeled as a set of n independent single-joint controllers. In this particular case, the focus is on controlling the shoulder joint actuator position of the *PUMA 560* manipulator using the schema illustrated in Figure 4. This scheme generates a command voltage u based on a desired joint trajectory, ensuring that the actual trajectory closely follows the reference. In this context, the proposed control system comprises an outer position loop, which provides the velocity reference, and an inner velocity loop, responsible for generating the torque command (Bacac et al., 2014; Lino et al., 2019; Singh et al., 2020).

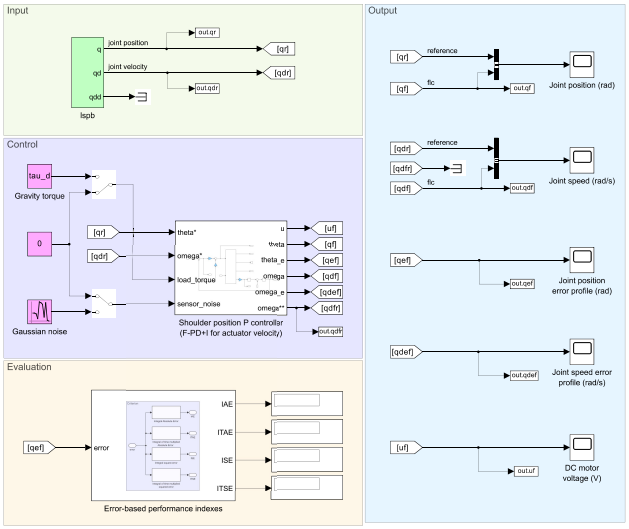

Figure 4: System block diagram

Thus, the output of the outer position loop, which has a proportional gain K_{pp} equal to 40,000 and a feedforward gain K_{ff} equal to 1, becomes the setpoint ω^* for the inner velocity loop. The latter responds more rapidly and manages setpoint changes and high-frequency load disturbances.

3.1. Fuzzy controller design

The inputs to the fuzzy PID controller are the error (proportional action), the change in error (derivative action), and the accumulated error (integral action). In this work, we apply a fuzzy PD (F-PD) controller combined with a separate linear controller that provides the integral action to eliminate steady-state error, thereby reducing the number of fuzzy rules. The control signal is the sum of the output from the F-PD controller and the integral of the error. The fuzzy inference system (FIS) employed is of the Mamdani type (Mamdani, 1974).

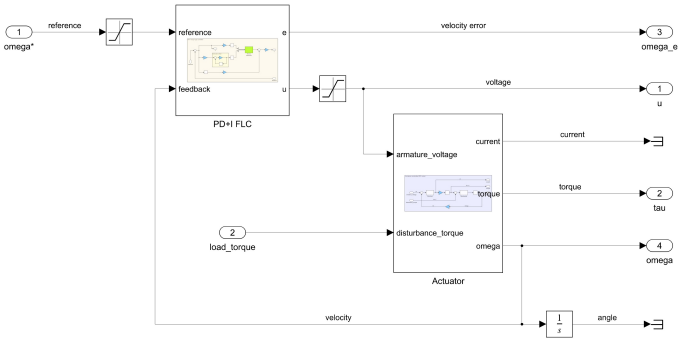

Figure 5: Inner control loop

The role of the gains $K_e = 4.4954$, $K_{ie} = 1634.8414$ and $K_{ce} = 0.002937$ in a fuzzy logic controller (FLC) is the same as in a conventional controller. As shown in Figure 5, both the input to the control loop and the output of the fuzzy controller have been saturated to the physical limits imposed by the nature of the system being controlled. Likewise, Figure 6 highlights the application of a low-pass filter (LPF) in the derivative with a gain of $N = 3.71905e{+}5$.

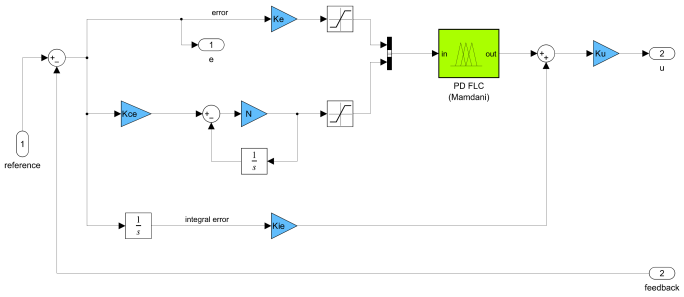

Figure 6: Fuzzy PD+I controller (F-PD+I)

3.1.1. *Fuzzification*

Once the inputs have been defined within the universe of discourse $[-300, 300]$, they must be transformed from a set of crisp values into fuzzy ones. To achieve this, three linguistic variables - namely *Negative*, *Zero*, and *Positive* - are used for the membership functions (MF). Specifically, two trapezoidal and one triangular MFs are used for each input signal.

For the output u, the same MFs used for the input variables are employed (Alavandar and Nigam, 2008), but with the universe of discourse (UOD) adjusted to the interval $[-40, 40]$.

The nine fuzzy rules which result from its Fuzzy Associative Matrix (FAM) take the form "'if $e(t)$ is A_i and $ce(t)$ is B_i, then $u(t)$ is C_i"', where A_i, B_i, and C_i are fuzzy sets defined by the linguistic labels *Negative*, *Zero* and *Positive*.

The centroid method is used for defuzzification. Additionally, during the aggregation stage, the *max* function is employed, while the implication step uses the *min* function.

4. Results and discussion

For the simulation, an LSPB trajectory is considered, moving the *PUMA 560* shoulder joint from an initial position of 0 to 1 rad in one second, with a sampling rate of 1000 Hz.

In order to evaluate the system response, a set of quality metrics has been employed — namely, the *Mean Absolute Error* (MAE), *Root Mean Squared Error* (RMSE), *Peak Signal-to-Noise Ratio* (PSNR), and the *Structural Similarity Index Measure* (SSIM), along with several transient response characteristics, including rise time, settling time, transient time, overshoot, and undershoot. Time-domain error-based indices are also used: the *Integral Square Error* (ISE), *Integral Time Square Error* (ITSE), *Integral Absolute Error* (IAE), and *Integral Time Absolute Error* (ITAE) (Tan et al., 2004).

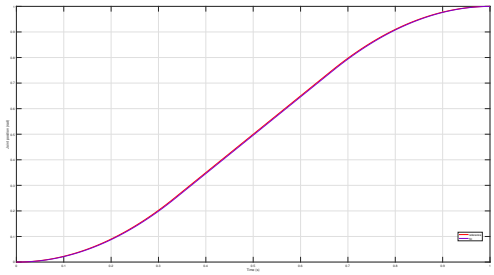

(a) Joint position

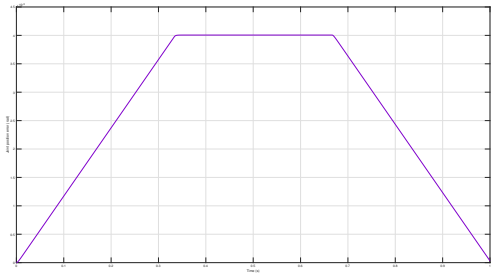

(b) Joint position error profile

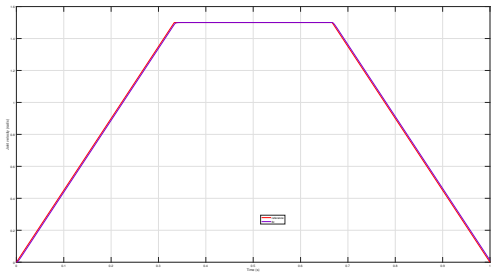

(c) Joint velocity

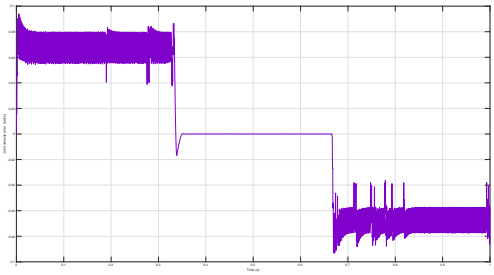

(d) Joint velocity error profile

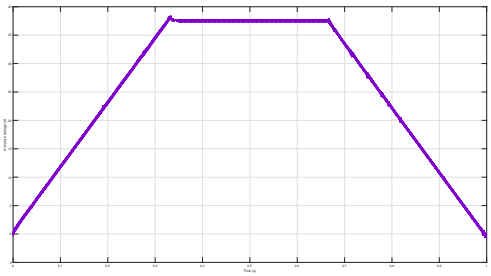

(e) Armature voltage

Figure 7: System response when no disturbance torque (τ_d) is applied

Second column in Table 1 presents the results of each metric, evaluated in the absence of linear disturbance τ_d. As shown in Figure 4, the response is satisfactory overall. Although a slight steady-state error is present, the system successfully meets the requirements imposed by the trajectory generator.

Table 1: Controller performance

Cost function	P/F-PD+I (no τ_d)	P/F-PD+I (with τ_d)
MAE	0.0027	0.0027
RMSE	0.0030	0.0030
PSNR	50.5037 dB	50.5022 dB
SSIM	0.9998	0.9998
Rise time (t_r)	0.5784 s	0.5784 s
Transient time	0.9084 s	0.9084 s
Settling time (t_s)	0.9084 s	0.9084 s
Settling min.	0.9 rad	0.9 rad
Settling max.	1 rad	1 rad
Overshoot	0 %	0%
Undershoot	0 %	0.000102 %
Peak	1 rad	1 rad
Peak time (t_p)	1 s	1 s
IAE	0.00267	0.00267
ITAE	0.001342	0.001342
ISE	8.913e−6	8.913e−6
ITSE	4.479e−6	4.481e−6

4.1. Disturbance torque effect

After accounting for the effect of gravitational torque on the joint, a disturbance torque τ_d was applied to q_2. This disturbance corresponds to half the maximum gravitational load observed at the joint (20 N·m), yielding 0.1855 N·m after reduction by the joint's gearbox ratio G. The inclusion of this disturbance leads to a slight decrease of 0.0030% in the PSNR compared to the undisturbed case. These results are summarized in the third column of Table 1. For a graphical illustration of the system trajectory under these conditions, see Figure 5.

5. CONCLUSIONS

This work presents a study on fuzzy control strategies for the cascaded position control of a DC motor, based on a detailed physical model of the *Unimation PUMA 560* shoulder joint actuator. The simulations were conducted in *Simulink*, and a comprehensive set of performance metrics was employed to rigorously evaluate the controller's tracking accuracy and its ability to reject input disturbances.

The control architecture was implemented as a cascaded structure, comprising an inner velocity loop and an outer position loop. The outer position controller was manually tuned, while the inner loop employed a fuzzy PD+I (F-PD+I) controller, with its parameters selected through trial and error. The results indicate that the fuzzy logic controller is well-suited for position control of the *PUMA 560* shoulder joint actuator.

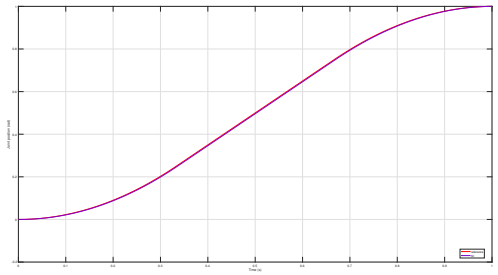

(a) Joint position

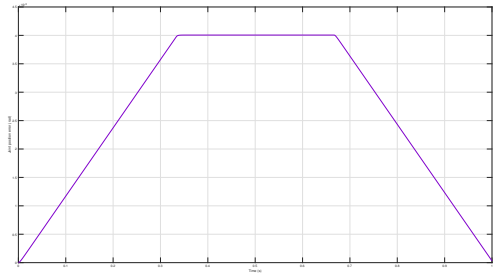

(b) Joint position error profile

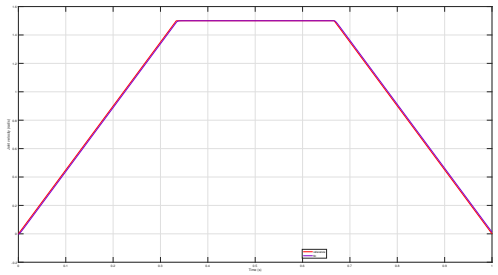

(c) Joint velocity

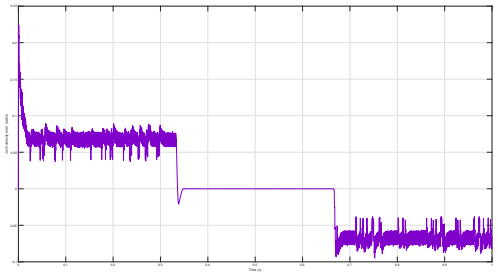

(d) Joint velocity error profile

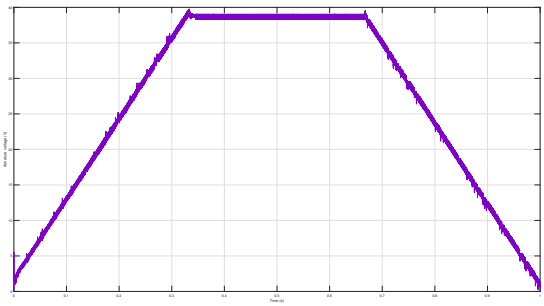

(e) Armature voltage

Figure 8: System response in presence of a $\tau_d = \frac{20}{G}$ `N.m`

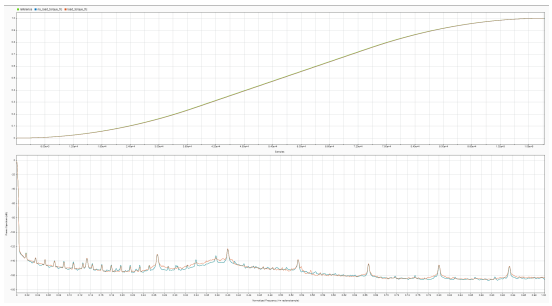

(a) Joint position

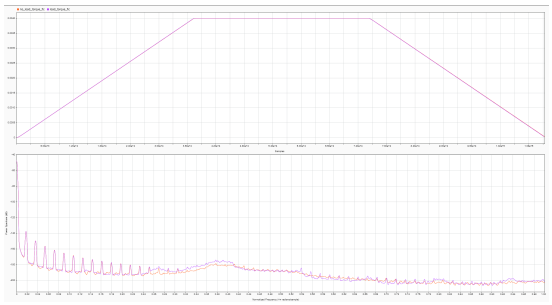

(b) Joint position error profile

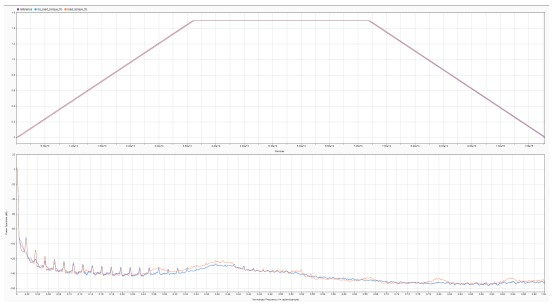

(c) Joint velocity

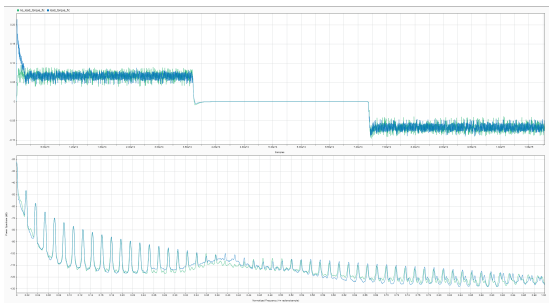

(d) Joint velocity error profile

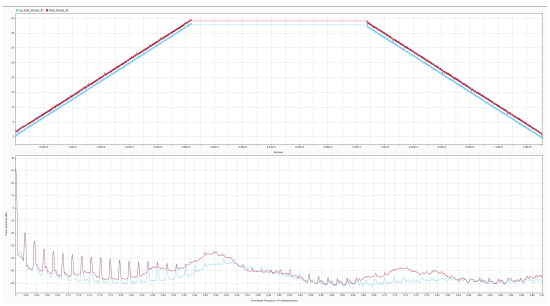

(e) Armature voltage

Figure 9: Control behavior in the previous scenarios. Time domain and frequency spectrum are shown at the top and bottom of each subfigure

Further research could focus on deploying the proposed control strategies onto a Programmable Logic Controller (PLC) or a *Field-Programmable Gate Array* (FPGA), thereby validating their practical applicability and robustness under real-world operating conditions.

References

Alavandar, S. and Nigam, M. J. (2008). Fuzzy PD+I control of a six DOF robot manipulator. *Industrial Robot: An International Journal*, 35(2):125–132.

Bacac, N., Slukic, V., Puskaric, M., Stih, B., Kamenar, E., and Zelenika, S. (2014). Comparison of different DC motor positioning control algorithms. In *2014 37th International Convention on Information and Communication Technology, Electronics and Microelectronics (MIPRO)*, pages 1654–1659. IEEE.

Barrientos, A., Peñin, L. F., Balaguer, C., and Aracil, R. (2007). *Fundamentos de robótica*. McGraw-Hill, second edition.

Corke, P. I. (2007). *Robotics, Vision and Control Fundamental Algorithms In MATLAB*. Springer, second edition.

Corke, P. I. and Armstrong-Helouvry, B. (1994). A search for consensus among model parameters reported for the PUMA 560 robot. In *Proceedings of the 1994 IEEE International Conference on Robotics and Automation*, pages 1608—1613. IEEE Comput. Soc. Press.

Lino, P., Konigsmarkova, J., and Maione, G. (2019). Feedback-Feedforward Position and Speed Control of DC Motors by Fractional-Order PI Controllers. In *2019 IEEE International Conference on Systems, Man and Cybernetics (SMC)*, pages 2584–2589. IEEE.

Mamdani, E. (1974). Application of fuzzy algorithms for control of simple dynamic plant. *Proceedings of the Institution of Electrical Engineers*, 121(12):1585.

Sierra-Garcia, J. E. and Santos, M. (2024). Agv fuzzy control optimized by genetic algorithms. *Logic Journal of the IGPL*, 32(6):955–970.

Singh, P., Kumar, V., and Rana, K. (2020). Speed Control of a Nonlinear DC Motor using Fuzzy PD + I Controller. In *2020 IEEE International Conference on Computing, Power and Communication Technologies (GUCON)*, pages 201–206. IEEE.

Tan, W., J. Marquez, H., and Chen, T. (2004). Performance Assessment of PID Controllers. *Control and Intelligent Systems*, 32(3).

Usoro, I. H., Itaketo, U. T., and Umoren, M. A. (2017). Control of a DC motor using fuzzy logic control algorithm. *Nigerian Journal of Technology*, 36(2):594.

Zadeh, L. A. (1996). *Fuzzy sets, fuzzy logic, and fuzzy systems*. Number v. 6 in Advances in fuzzy systems. World Scientific Pub. Co.